A Study on the Feasibility of Dual-Wavelength Radar for Identification of Hydrometeor Phases

LIANG LIAO

Goddard Earth Sciences and Technology Center, University of Maryland, Baltimore County, Greenbelt, Maryland

ROBERT MENEGHINI

NASA Goddard Space Flight Center, Greenbelt, Maryland

(Manuscript received 25 February 2010, in final form 3 September 2010)

ABSTRACT

An important objective for the dual-wavelength Ku-/Ka-band precipitation radar (DPR) that will be on board the Global Precipitation Measurement (GPM) core satellite is to identify the phase state of hydrometeors along the range direction. To assess this, radar signatures are simulated in snow and rain to explore the relation between the differential frequency ratio (DFR), defined as the difference of radar reflectivity factors between Ku and Ka bands, and the radar reflectivity factor at Ku band Z_{Ku} for different hydrometeor types. Model simulations indicate that there is clear separation between snow and rain in the Z_{Ku}–DFR plane assuming that the snow follows the Gunn–Marshall size distribution and rain follows the Marshall–Palmer size distribution. In an effort to verify the simulated results, the data collected by the Airborne Second-Generation Precipitation Radar (APR-2) in the Wakasa Bay Advanced Microwave Scanning Radiometer for Earth Observing System (AMSR-E) campaign are employed. Using the signatures of linear depolarization ratio at Ku band, the APR-2 data can be easily divided into the regions of snow, mixed phase, and rain for stratiform storms. These results are then superimposed onto the theoretical curves computed from the model in the Z_{Ku}–DFR plane. For over 90% of the observations from a cold-season stratiform precipitation event, snow and rain can be distinguished if the Ku-band radar reflectivity exceeds 18 dBZ (the minimum detectable level of the GPM DPR at Ku band). This is also the case for snow and mixed-phase hydrometeors. Although snow can be easily distinguished from rain and melting hydrometeors by using Ku- and Ka-band radar, the rain and mixed-phase particles are not always separable. It is concluded that Ku- and Ka-band dual-wavelength radar might provide a potential means to identify the phase state of hydrometeors.

1. Introduction

The Global Precipitation Measurement (GPM) mission has been proposed for mapping of precipitation globally following the success of the Tropical Rainfall Measuring Mission, which measures the precipitation in tropical and subtropical regions (Simpson et al. 1996; Kummerow et al. 2000; Kozu et al. 2001). The dual-wavelength precipitation radar (DPR) on board the GPM core satellite is expected to improve the accuracy of estimates of precipitation rate and also to enable the retrieval of microphysical properties of hydrometeors, such as particle size distribution and phase state. Because the GPM will fly in a higher orbital inclination (65°), the radar observations will be extended to mid- and high-latitude regions where both snow and rain frequently occur. Moreover, because the radar algorithms for estimates of precipitation rate and water content differ for snow and rain, it is necessary to study the feasibility of the GPM DPR for identification of hydrometeor phase state. This capability is also useful in convective rain where a clearly defined bright band is usually absent. Having knowledge of where regions of snow, rain and mixed-phase precipitation occur along the radar range direction is important in determining how to allocate estimates of total path attenuation as derived either by the radiometer or by the use of the radar surface reference technique (Meneghini et al. 2000). Although hydrometeor identification has been studied for polarimetric radar (Ryzhkov and Zrnic 1998; Liu and Chandrasekar 2000; Dolan and Rutledge 2009), such research has not yet been well

Corresponding author address: Dr. Liang Liao, Goddard Earth Science Technology/UMBC, Code 613.1, NASA/GSFC, Greenbelt, MD 20771.
E-mail: liang.liao-1@nasa.gov

DOI: 10.1175/2010JAMC2499.1

established using nonpolarimetric (copolarization) radar. Use of radar reflectivity at one frequency alone is not sufficient to distinguish snow from rain echoes because light to moderate rain exhibits a similar range of reflectivities as those of snow. However, the differential frequency ratio (DFR), which is defined as the difference of radar reflectivity factors between Ku and Ka bands, provides information that, together with Ku-band radar reflectivity, can be useful in improving the capability to distinguish snow and rain.

To explore the capability of the GPM DPR for separation of snow and rain, we start with simulations of radar signatures at the DPR frequencies (Ku and Ka bands with frequencies of 13.6 and 35.5 GHz, respectively) in snow and rain in an effort to find distinctive characteristics based on assumed particle size distributions. To check the model simulations we use radar measurements taken by the Airborne Second-Generation Precipitation Radar (APR-2) during the Wasaka Bay Advanced Microwave Scanning Radiometer for Earth Observing System (AMSR-E) field campaign in 2003 over the Sea of Japan on board a National Aeronautics and Space Administration (NASA) P-3 aircraft (Im 2003; Sadowy et al. 2003). The APR-2, operating at approximately the same frequencies as the DPR, is also capable of obtaining the linear depolarization ratio (LDR) at Ku band in addition to the measurements of radar reflectivity factors and Doppler velocities at Ku and Ka bands. The LDR provides information that can be used to identify accurately the mixed-phase region in stratiform storms, with which the radar data can be easily divided into frozen, melting, and liquid regions. The radar measurements from these regions are then compared with the model computations. Thus, the potential to separate hydrometeors among three different phases can be effectively studied.

This paper is organized as follows. In section 2, simulations of the Ku- and Ka-band radar in snow and rain are performed using the assumed particle size distributions. This is followed by a description of APR-2 measurements during the Wasaka Bay field campaign in section 3. The capability of the Ku- and Ka-band dual-wavelength radar to distinguish phase states of hydrometeors is analyzed in section 4 using measured radar data. A summary is given in section 5.

2. Dual-wavelength radar simulations

Simulation of dual-wavelength radar signatures in snow and rain provides an important means to examine the distinctive features of radar signals from which the phase states of hydrometeors can be possibly identified. What follows is a brief description of the radar parameters involved in this study.

The effective radar reflectivity factor Z_e, which is related to the particle size distribution $N(D)$ and the backscattering cross section $\sigma_b(D, \lambda)$ of the hydrometeors for an incident wavelength λ, is given as

$$Z_e = \frac{\lambda^4}{\pi^5 |K_w|^2} \int_0^\infty N(D)\sigma_b(D, \lambda)\, dD, \tag{1}$$

where the the dielectric factor K_w is used to designate $(m^2 - 1)/(m^2 + 2)$, with m being the complex refractive index of water. By convention, $|K_w|^2$ is taken to be 0.93 (Battan 1973). Whereas Z_e can be obtained from the radar return power, $\sigma_b(D, \lambda)$ for spheres can be directly computed from Mie theory. Note that for snow, which is a mixture of air and ice, its effective dielectric constant is computed by the Bruggeman (1935) mixing equation. The radar DFR in decibels, describing the difference of the radar reflectivity at 2 wavelengths, is defined as

$$\mathrm{DFR} = 10 \log(Z_u/Z_v), \tag{2}$$

where Z_u and Z_v are the radar reflectivity factors at wavelengths λ_u and λ_v. In this paper, λ_u is associated with the longer wavelength corresponding to the lower frequency (Ku band). Particle shapes of snow, mixed phase, and rain are assumed to be spheres.

For convenience, the hydrometeor size distribution is often parameterized by an analytical form based on measured particle size spectra. The most common particle size distributions are the exponential, gamma, and lognormal distributions with 2 or 3 characteristic parameters in the function (Bringi et al. 2002; Gorgucci et al. 2000, 2002; Tian et al. 2010). It is known, under atmospheric equilibrium conditions, that the raindrop size distribution is represented well by the exponential relation—namely, the Marshall–Palmer distribution (Marshall and Palmer 1948), which is expressed as

$$N(D) = N_0 e^{-\Lambda D} \tag{3}$$

where

$$N_0 = 8000\,(\mathrm{m}^{-3}\,\mathrm{mm}^{-1}) \quad \text{and} \tag{4}$$

$$\Lambda = 4.1 R^{-0.21}\,(\mathrm{mm}^{-1}). \tag{5}$$

Here $N(D)\Delta D$ is the number concentration of the raindrops with diameters in the range D to $D + \Delta D$ and R is the rainfall rate in millimeters per hour. For snow it has been found that the size distribution of aggregate snowflakes also yields (3) (Gunn and Marshall 1958) but with

$$N_0 = 3.8 \times 10^3 R^{-0.87}\,(\mathrm{m}^{-3}\,\mathrm{mm}^{-1}) \quad \text{and} \tag{6}$$

$$\Lambda = 2.55 R^{-0.48}\,(\mathrm{mm}^{-1}). \tag{7}$$

The diameter D in (3) refers to the melted diameter of the snowflake. To compute the backscattering cross section of snowflakes in (1), the melted size diameter must be converted to the actual diameter of the snowflake, which is a mixture of ice and air. Transformation of the snow particles from their melted to actual size depends solely on the snow mass density. Many observations indicate that snow density ρ_s is inversely proportional to particle size (Mitchell et al. 1990; Brown and Francis 1995; Heymsfield et al. 2004; Wang et al. 2005; Brandes et al. 2007) and can be expressed in power-law form; that is,

$$\rho_s(D) = \alpha D^{\beta}, \tag{8}$$

where α and β are coefficients that are to be determined from observation. We hereinafter refer to the snow density as variable snow density if it depends on particle size. Because of the considerable variation in the density–size relations, which depends on snow type, amount of riming, and other conditions under which the studies are undertaken, it is convenient to use the average bulk density $\overline{\rho}_s$ (or fixed snow density), which is independent of particle size. The average bulk density of snow can be defined as the ratio of mass content to the total volume of the hydrometeor:

$$\overline{\rho}_s = \frac{\int \rho_s(D) D^3 N(D)\, dD}{\int D^3 N(D)\, dD}. \tag{9}$$

Figure 1 shows the simulated radar signatures in the Z_{Ku}–DFR plane for different values of fixed and variable snow density. In these simulations the snow size distribution is assumed to be the Gunn–Marshall relation (Gunn and Marshall 1958) and the rain is assumed to follow the Marshall–Palmer raindrop size distribution (Marshall and Palmer 1948) described previously. As shown in the results for the case of fixed snow density (Fig. 1a), there is a clear separation between regions of snow (blue) and rain (red) in the Z_{Ku}–DFR space. Departures of the radar signatures from snow to rain grow quickly as the snow density decreases, evidenced by the results of the snow densities with values varying from 0.05 to 0.5 g cm^{-3}; these separations become increasingly pronounced as the Ku-band radar reflectivity increases. For reference, the curves of constant rain rate (black) are also plotted. For snow these should be interpreted as the equivalent rain rate, which is computed from the velocity–size

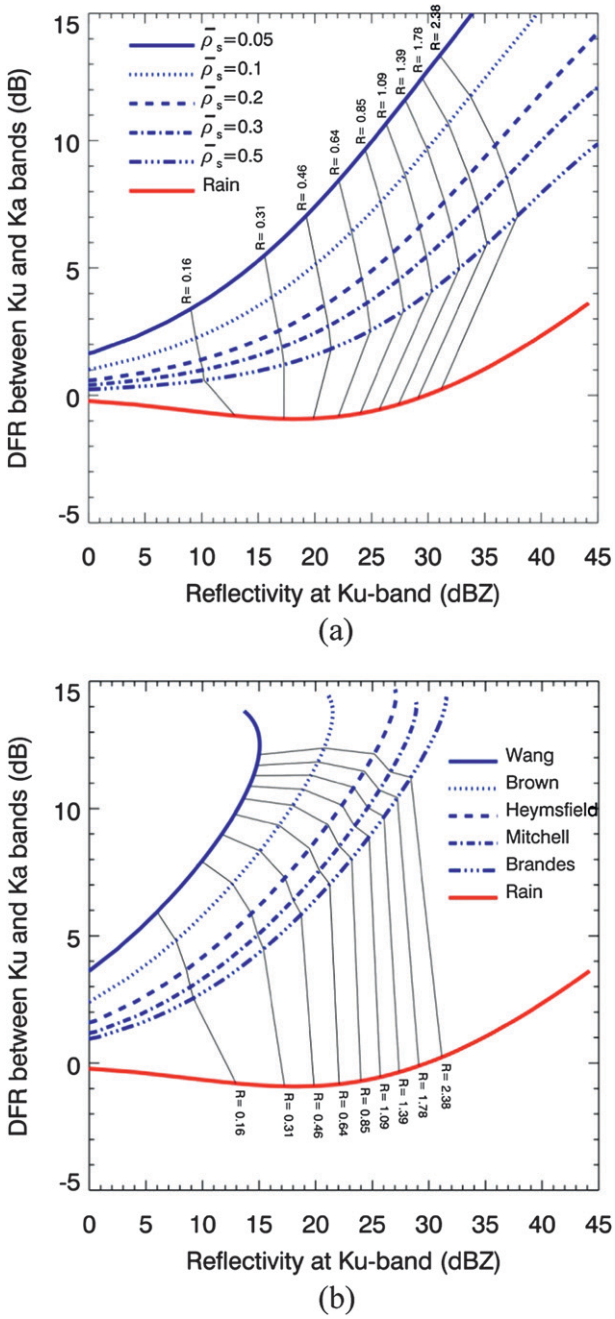

FIG. 1. Theoretical relationships between DFR and radar reflectivity factor at Ku band for snow (blue curves) and rain (red curves) as computed from assumed particle size distributions. The black contour lines correspond to equivalent rain rate R (mm h^{-1}). (a) Fixed snow density ($\overline{\rho}_s$). (b) Variable snow density as expressed as a function of particle size and as obtained from the empirical relations from Brown and Francis (1995), Wang et al. (2005), Heymsfield et al. (2004), Brandes et al. (2007), and Mitchell et al. (1990).

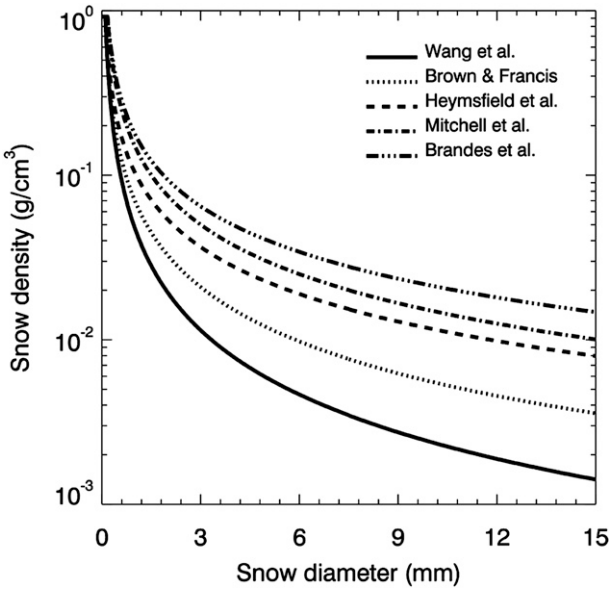

FIG. 2. Snow density as a function of particle size as obtained from the empirical relations obtained by Brown and Francis (1995), Wang et al. (2005), Heymsfield et al. (2004), Brandes et al. (2007), and Mitchell et al. (1990).

relation reported by Langleben (1954). In a similar manner, the results of the variable snow density are depicted in Fig. 1b where several empirical density–size relations from the results of Wang et al. (2005), Brown and Francis (1995), Heymsfield et al. (2004), Mitchell et al. (1990), and Brandes et al. (2007) are shown as derived from the snow density–size relations plotted in Fig. 2. As in the case of constant snow density, the results clearly show that the regions of snow and rain can be separated. However, in the variable-density case, the separation is much larger than in the case of fixed snow density. The results shown in Fig. 1 are promising in that they suggest a clear separation between snow and rain returns in the Z_{Ku}–DFR plane. However, these results need to be confirmed by using actual radar measurements. This will be a focus of the remainder of the paper.

3. APR-2 radar measurements

In support of the NASA GPM mission, NASA Jet Propulsion Laboratory (JPL) has built the APR-2 as a prototype for advanced dual-frequency spaceborne radar that emulates the GPM core satellite's Ku- and Ka-band radar (Sadowy et al. 2003). The APR-2 is capable of making simultaneous measurements of co- and cross-polarized reflectivity factors and Doppler velocities at the frequencies of 13.4 GHz (Ku band) and 35.6 GHz (Ka band). In January and February 2003 the APR-2 on board a NASA P-3 aircraft was deployed to the Wakasa Bay AMSR-E validation site over the Sea of Japan (Im 2003). During 12 flights and with more than 30 h of measurements, the APR-2 collected valuable datasets for the study of precipitation systems, including snow and rain events, over both land and ocean.

Figure 3 illustrates the measurements of the APR-2 at nadir from a stratiform storm during the Wakasa Bay

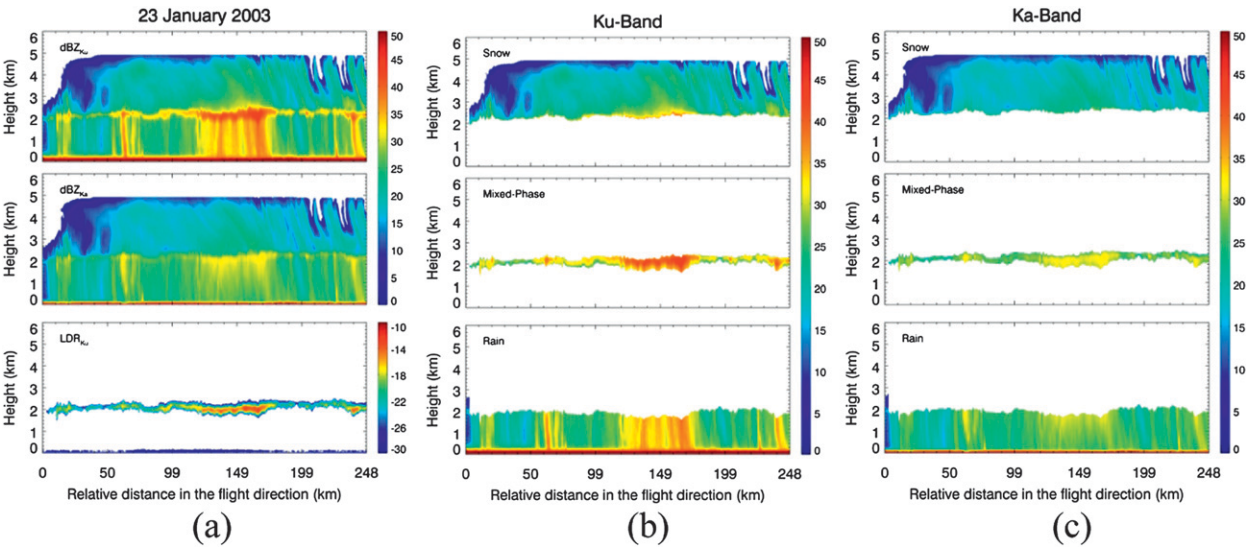

FIG. 3. Measurements taken from the APR-2 during the Wakasa Bay AMSR-E field campaign on 23 Jan 2003. (a) Radar reflectivity factors at (top) Ku band and (middle) Ka band and (bottom) LDR at Ku band. (b) Radar reflectivity factors at Ku band that are broken down into the regions of (top) snow, (middle) mixed phase, and (bottom) rain based on the Ku-band LDR. (c) Radar reflectivity factors at Ka band that are broken down into the regions of (top) snow, (middle) mixed phase, and (bottom) rain based on the Ku-band LDR.

field campaign on 23 January 2003. The radar reflectivity factors shown in the left columns (Fig. 3a) correspond to the Ku (top panel) and Ka bands (middle panel). With a fine-range resolution (30 m), the bright band is clearly defined at an altitude around 2 km from the surface that is identified by a strong, narrow band. The LDR measured at Ku band (bottom panel) effectively identifies the mixed-phase region, which can be used to divide the measurements into regions of snow, melting, and rain. This is based on the fact that higher LDR is associated with melting particles (Kumagai et al. 1993; Meneghini and Kumagai 1994; Brandes and Ikeda 2004). A threshold of −25 dB for LDR, that is, LDR ≥ −25 dB, is chosen for identification of the mixed-phased region. Figures 3b and 3c show, respectively, the Ku- and Ka-band radar data that correspond to snow (top), mixed phase (middle), and rain (bottom). Using the radar measurements associated with hydrometeors with different phases in combination with the model simulations described in section 3, the capability of the Ku- and Ka-band radar technique can be tested to differentiate the phase states of the hydrometeors.

4. Ku- and Ka-band radar phase identification

To test whether the radar measurements can be used to separate the regions of snow, mixed phase, and rain, as indicated by the radar simulations, we superimpose the radar data onto the theoretical model computations in the plane of DFR and Ku-band radar reflectivity factor. Shown in Fig. 4 are the scatterplots of the radar data that overlay the simulated curves that are respectively computed at fixed snow densities (Fig. 4a) and variable snow density (Fig. 4b). The data points in blue, green, and red represent measurement results for the regions of snow, mixed phase, and rain, respectively, acquired from the APR-2 measurements in stratiform rain on 23 January 2003 shown in Fig. 3. For results from the theoretical computations for rain are given by a heavy solid line, while the snow results are depicted by several thin curves that are associated with either different snow densities (Fig. 4a) or different density–size relations (Fig. 4b). Comparison of the radar measurements with the model simulations in snow for the fixed and variable snow densities reveals that the radar simulations are in much better agreement if the averaged bulk (or fixed) snow density is used. We therefore confine our discussion to the case of the fixed snow density hereinafter. It is evident that the majority of the snow and rain echoes are consistent with the model simulations. However, a few data points of snow slip into negative region of DFR when the Ku-band radar reflectivity factors are in the range from 10 to 15 dBZ.

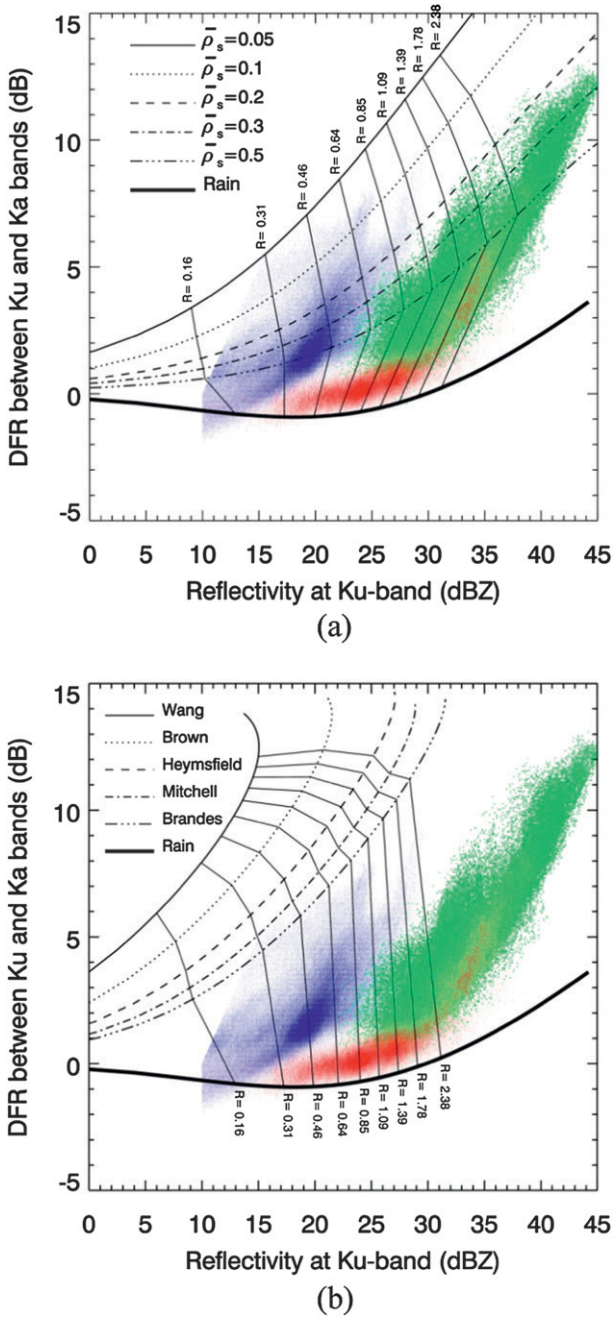

FIG. 4. Scatterplots of the APR-2 data for snow (blue), mixed phase (green), and rain (red) that are superimposed on the theoretical curves computed by the (a) fixed snow density and (b) variable snow density. Note that the total numbers of data points are 565 713, 75 032, and 367 234 for snow, mixed phase, and rain, respectively.

These results contradict theoretical calculations (Liao et al. 2005, 2008) showing that the DFR is always greater than zero for snow. These negative DFR occurrences are probably the result of sampling errors (from a finite number of samples) and from low signal-to-noise ratios.

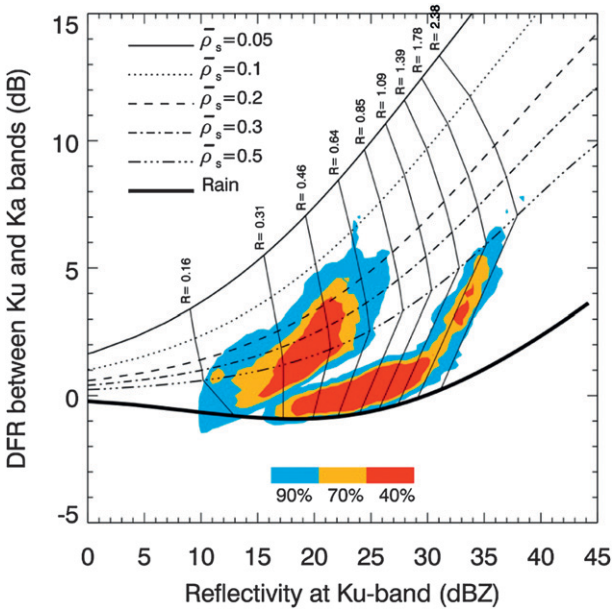

FIG. 5. Two-dimensional PDF for snow (upper cluster) and rain (lower cluster) as the contours of data populations are plotted at 40%, 70%, and 90%.

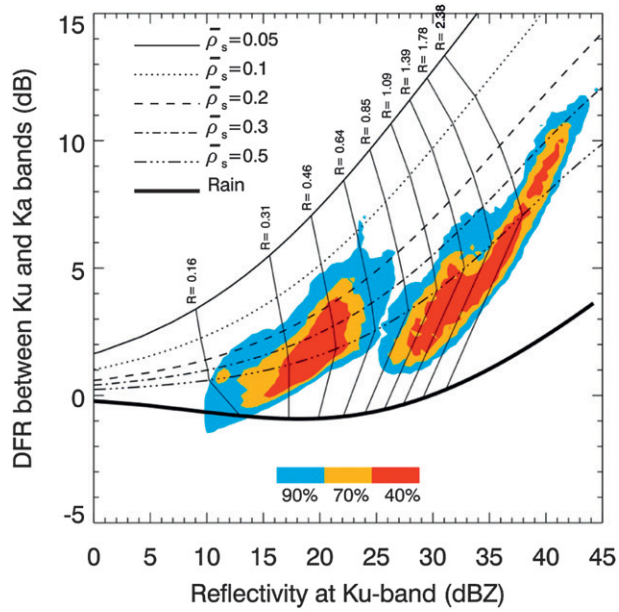

FIG. 6. As in Fig. 5, but for snow (left cluster) and mixed phase (right cluster).

Note that the data points shown in Fig. 4 include all of the measurements of the APR-2 (from 23 equally spaced angle bins), covering a cross-track scan ±25° from nadir. In addition, a simple attenuation correction procedure for rain has been taken into account in the dataset using the surface reference technique (SRT; Meneghini et al. 2000). Snow attenuation, on the other hand, can be generally ignored for a downward-looking radar. Attenuation in the melting layer can be corrected based on a melting-layer model (e.g., Liao and Meneghini 2005b; Liao et al. 2009). However, because the rain height is relatively shallow (about 2 km), and also because of relatively weak reflectivities for most of the measurements, attenuation correction seems to have little effect on the results shown in Fig. 4.

A quantitative analysis of the results can be made by computing two-dimensional probability density functions (PDF) from the data. Figure 5 exhibits the PDF results in the Z_{Ku}–DFR space for snow (upper cluster) and rain (lower cluster). For the sake of comparison, the contours of the PDF that enclose data populations at levels of 40%, 70%, and 90% are plotted. As shown in Fig. 5, in at least 70% cases, rain and snow are completely separated; for those contours that contain 90% of the data, the rain and snow regions can be fully distinguished if the Ku-band reflectivity exceeds 18 dBZ (which is approximately the DPR minimum detectable level at Ku band). Similar comparisons of the PDFs are shown in Fig. 6 between the snow and mixed-phase data. We find that 90% of the data from snow and mixed phase are separable. This finding, along with those from Fig. 5, suggests that the snow returns usually can be differentiated from rain and mixed-phase returns by using measurements of DFR and Ku-band radar reflectivity. In contrast, however, the returns from rain cannot always be distinguished from mixed-phase cases when the Ku-band radar reflectivity factors are in the range from 25 to 35 dBZ, as illustrated in Fig. 7. This overlap region is associated with the trailing part of the melting layer in which rain and melting snow returns yield approximately the same magnitudes of DFR and radar reflectivity factor at Ku band. For values of Z_{Ku} below 25 dB the returns are exclusively associated with rain, whereas above 35 dB the returns are primarily associated with the mixed-phase region. These findings are supported by similar comparisons (not shown) from data acquired from other flights on different days. As such, the results derived from this case are representative of other stratiform events observed during the Wakasa Bay field campaign.

5. Summary

To develop an algorithm for the Ku- and Ka-band dual-wavelength spaceborne radar for the identification of hydrometeor phase state, such as snow, melting snow (mixed phase), and water, we start with model simulations that are focused on snow and rain. Because the rain and snow particle size distributions are respectively described by the Marshall–Palmer and Gunn–Marshall

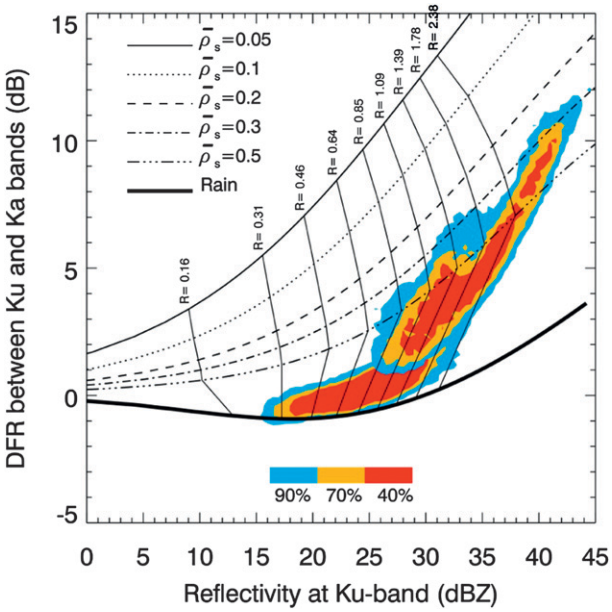

FIG. 7. As in Fig. 5, but for rain (lower-left cluster) and mixed phase (upper-right cluster).

exponential functions, theoretical computations of the relations between DFR and radar reflectivity factor at Ku band are performed using both a constant snow density (invariant with particle size) and variable snow density (size dependent). It is shown that snow and rain can usually be clearly distinguished in the Z_{Ku}–DFR plane. The data taken from the NASA JPL APR-2 Ku- and Ka-band airborne radar during the Wakasa Bay experiment are employed to check the model simulations and also to assess the feasibility of the dual-wavelength radar technique for identification of hydrometeor phase. Having superimposed the data collected in stratiform rain on 23 January 2003 onto the theoretical curves in the plane of DFR and radar reflectivity at Ku band, it is found that the radar measurements are generally consistent with the model simulations for snow and rain. When compared with measurements, better agreement is obtained by using fixed snow density than by using variable snow density. Note that the simulated radar signatures would have changed had different model assumptions been used, such as particle size distribution, particle shape, and orientation (Matrosov 2007). Analysis of the two-dimensional PDF of the data from snow, rain, and mixed phase indicates that snow can be easily distinguished from rain and mixed-phase hydrometeors if the radar reflectivity factor at Ku band is greater than 18 dBZ. Rain, however, is not always separable from mixed-phase data. In stratiform rain, the region of overlap occurs at ranges near the lower boundary of the melting layer where the snow melting is nearly complete and where the radar reflectivities and DFR values from the melting snow resemble those from rain. Apart from this overlap region ($25 < Z_{\mathrm{Ku}} < 35$ dBZ), the separation between the regions of rain and mixed phases appears feasible.

Although the radar technique described in this study presents a promising way to separate the regions of snow, rain, and mixed-phase hydrometeors, attenuation due to rain and mixed-phase particles may complicate the identification because Ka band experiences much more attenuation than the Ku band in general, resulting in an increase in the DFR. Without proper attenuation correction, it is possible to misclassify the hydrometeors. One way to circumvent this problem is to use the SRT and dual-wavelength radar retrieval algorithms. The SRT provides an effective means for attenuation correction at the surface based on the difference of surface returns between rain and rain-free areas. The dual-wavelength radar backward approach that works on a gate-by-gate basis can possibly be incorporated with the phase identification scheme to identify the phase states beginning from the surface and moving upward toward the storm top (Liao and Meneghini 2005a; Liao et al. 2008). To develop a fully functional radar algorithm, an investigation into an optimal selection of the DFR–Z(Ku) relation that effectively separates different phase regions is needed. To achieve this, a further study will be undertaken that includes an analysis of dual-wavelength radar measurements and the model computations linking DFR to radar reflectivity under various microphysical conditions, as well as an exploration of convective storms in which an obvious bright band is absent. In addition, the study will be carried out to account for possible impacts resulting from relatively coarse range resolution (125 m) of the GPM DPR as opposed to the APR-2 (30 m). The development of an effective dual-wavelength method to distinguish the rain, snow, and mixed-phase hydrometeors will be an important step toward an accurate, efficient DPR profiling algorithm.

Acknowledgments. The authors thank Dr. Eastwood Im and Dr. Simone Tanelli of the NASA Jet Propulsion Laboratory for providing the APR-2 radar data and the processing software. This work is supported by Dr. R. Kakar of NASA Headquarters under NASA's Precipitation Measurement Mission (PMM) Grant NNH06ZDA001N-PMM.

REFERENCES

Battan, L. J., 1973: *Radar Observation of the Atmosphere*. University of Chicago, 324 pp.

Brandes, E., and K. Ikeda, 2004: Freezing-level estimation with polarimetric radar. *J. Appl. Meteor.,* **43,** 1541–1553.

——, ——, G. Zhang, M. Schoenhuber, and R. Rasmussen, 2007: A statistical and physical description of hydrometeor distributions in Colorado snowstorms using a video disdrometer. *J. Appl. Meteor. Climatol.,* **46,** 634–650.

Bringi, V., G. Huang, V. Chandrasekar, and E. Gorgucci, 2002: A methodology for estimating the parameters of a gamma raindrop size distribution model from polarimetric radar data: Application to a squall-line event from the TRMM/Brazil campaign. *J. Atmos. Oceanic Technol.,* **19,** 633–645.

Brown, P. R. A., and P. N. Francis, 1995: Improved measurement of the ice water content in cirrus using a total-water probe. *J. Atmos. Oceanic Technol.,* **12,** 1679–1688.

Bruggeman, D. A. G., 1935: Berechnung verschiedener physikalischer Konstanten von heterogenen Substanzen: I. Dielectrizitatskonstanten und Leitfahigkeiten der Mischkorper aus isotropen Substanzen (Calculation of various physical constants of heterogeneous substance: I. Dielectric constants and conductivity of the heterostructure from isotropic substances). *Ann. Phys.,* **24,** 636–679.

Dolan, B., and S. A. Rutledge, 2009: A theory-based hydrometeor identification algorithm for X-band polarimetric radars. *J. Atmos. Oceanic Technol.,* **26,** 2071–2088.

Gorgucci, E., G. Scarchilli, V. Chandrasekar, and V. Bringi, 2000: Measurement of mean raindrop shape from polarimetric radar observations. *J. Atmos. Sci.,* **57,** 3406–3413.

——, ——, ——, and ——, 2002: Estimation of raindrop size distribution parameters from polarimetric radar measurements. *J. Atmos. Sci.,* **59,** 2373–2384.

Gunn, K. L. S., and J. S. Marshall, 1958: The distribution with size of aggregate snowflakes. *J. Meteor.,* **15,** 452–461.

Heymsfield, A. J., A. Bansemer, P. R. Field, C. Schmitt, C. Twohy, and M. R. Poellot, 2004: Effective ice particle densities from aircraft data. *J. Atmos. Sci.,* **61,** 982–1003.

Im, E., 2003: APR-2 dual-frequency airborne radar observations, Wakasa Bay. National Snow and Ice Data Center, Boulder, CO, digital media. [Available online at http://nsidc.org/data/nsidc-0195.html.]

Kozu, T., and Coauthors, 2001: Development of precipitation radar onboard the Tropical Rainfall Measuring Mission (TRMM) satellite. *IEEE Trans. Geosci. Remote Sens.,* **39,** 102–116.

Kumagai, H., R. Meneghini, and T. Kozu, 1993: Preliminary results from multiparameter airborne rain radar measurement in the western Pacific. *J. Appl. Meteor.,* **32,** 431–440.

Kummerow, C., and Coauthors, 2000: The status of the Tropical Rainfall Measuring Mission (TRMM) after two years in orbit. *J. Appl. Meteor.,* **39,** 1965–1982.

Langleben, M. P., 1954: The terminal velocity of snowflakes. *Quart. J. Roy. Meteor. Soc.,* **80,** 174–181.

Liao, L., and R. Meneghini, 2005a: A study of air/space-borne dual-wavelength radar for estimates of rain profiles. *Adv. Atmos. Sci.,* **22,** 841–851.

——, and ——, 2005b: On modeling air/spaceborne radar returns in the melting layer. *IEEE Trans. Geosci. Remote Sens.,* **43,** 2799–2809.

——, ——, T. Iguchi, and A. Detwiler, 2005: Use of dual-wavelength airborne radar for snow parameter estimation. *J. Atmos. Oceanic Technol.,* **22,** 1494–1506.

——, ——, L. Tian, and G. M. Heymsfield, 2008: Retrieval of snow and rain from combined X- and W-band airborne radar measurements. *IEEE Trans. Geosci. Remote Sens.,* **46,** 1514–1524.

——, ——, ——, and ——, 2009: Measurements and simulations of nadir-viewing radar returns from the melting layer at X- and W-bands. *J. Appl. Meteor. Climatol.,* **48,** 2215–2226.

Liu, H., and V. Chandrasekar, 2000: Classification of hydrometeors based on polarimetric radar measurements: Development of fuzzy logic and neuro-fuzzy systems, and in situ verification. *J. Atmos. Oceanic Technol.,* **17,** 140–164.

Marshall, J. S., and W. M. Palmer, 1948: The distribution of raindrops with size. *J. Meteor.,* **5,** 165–166.

Matrosov, S. Y., 2007: Modeling backscatter properties of snowfall at millimeter wavelengths. *J. Atmos. Sci.,* **64,** 1727–1736.

Meneghini, R., and H. Kumagai, 1994: Characteristics of the vertical profiles of dual-frequency, dual-polarization radar data in stratiform rain. *J. Atmos. Oceanic Technol.,* **11,** 701–711.

——, T. Iguchi, T. Kozu, L. Liao, K. Okamoto, J. A. Jones, and J. Kwiatkowski, 2000: Use of the surface reference technique for path attenuation estimates from TRMM precipitation radar. *J. Appl. Meteor.,* **39,** 2053–2070.

Mitchell, D. L., R. Zhang, and R. L. Pitter, 1990: Mass-dimensional relations for ice particles and the influence of riming on snowfall rates. *J. Appl. Meteor.,* **29,** 153–163.

Ryzhkov, A. V., and D. S. Zrnic, 1998: Discrimination between rain and snow with a polarimetric radar. *J. Appl. Meteor.,* **37,** 1228–1240.

Sadowy, G. A., A. C. Berkun, W. Chun, E. Im, and S. L. Durden, 2003: Development of an advanced airborne precipitation radar. *Microwave J.,* **46,** 84–98.

Simpson, J., C. Kummerow, W.-K. Tao, and R. F. Adler, 1996: On the Tropical Rainfall Measuring Mission (TRMM). *Meteor. Atmos. Phys.,* **60,** 19–36.

Tian, L., G. M. Heymsfield, A. Heymsfield, L. Li, C. H. Twohy, and R. C. Srivastava, 2010: A study of cirrus ice particle distribution using TC4 observations. *J. Atmos. Sci.,* **67,** 195–216.

Wang, Z., G. M. Heymsfield, L. Li, and A. J. Heymsfield, 2005: Retrieval optically thick ice cloud microphysical properties by using airborne dual-wavelength radar measurements. *J. Geophys. Res.,* **110,** D19201, doi:10.1029/2005JD005969.